Applied Surface Science 629 (2023) 157439

Contents lists available at ScienceDirect

Applied Surface Science

journal homepage: www.elsevier.com/locate/apsusc

Full Length Article

Surface hardening of extreme ultraviolet(EUV) photoresist by CS_2 plasma for highly selective and low damage patterning

Won Jun Chang [a], Hee Ju Kim [a], Geun Young Yeom [a,b,*]

[a] School of Advanced Materials Science and Engineering, Sungkyunkwan University, Suwon 440-746, Republic of Korea
[b] SKKU Advanced Institute of Nano Technology (SAINT), Sungkyunkwan University, Suwon 440-746, Republic of Korea

ARTICLE INFO

Keywords:
Extreme ultraviolet (EUV)
Photoresist
CS_2 plasma
Hardening
Annealing
Line edge roughness (LER)

ABSTRACT

Extreme ultraviolet (EUV) lithography has the advantage of implementing a finer pattern by using a wavelength of 13.5 nm light source with a higher resolution value than the existing ArF light source. However, there are several issues regarding EUV photoresist (PR), such as low etch resistance due to thin thickness and pattern mismatch during subsequent processing/deterioration of electrical characteristics of the device due to increase in line edge roughness (LER). In this study, the effect of CS_2 plasma treatment and/or followed annealing at 80 °C on the EUV PR properties was investigated to improve PR characteristics such as LER, etch resistance, etc. during the etching by CF_4 plasma. The CS_2 plasma treatment and followed annealing improved the PR characteristics such as decreased ΔLER, decreased ΔCritical dimension, and decreased ΔThickness of the PR after the etching compared to the reference and/or annealed PR. Especially, the PR treated by CS_2 plasma + annealing showed the improvement of etch resistance of ~ 70 % compared to the reference PR. The X-ray photoelectron spectroscopy and Fourier transform infrared spectroscopy showed that the improvement of EUV PR properties were related to the formation of C—S, O═S bonds on the surface of PR by the CS_2 plasma treatment + annealing.

1. Introduction

The lithography technology for the nanoscale patterns of 10 nm or less is being replaced by the extreme ultraviolet (EUV) lithography technology from the multi-patterning technology through ArF immersion lithography.[1–4] Since the existing multi-patterning technology using ArF immersion lithography has gradually reached its limit[5–8], EUV lithography technology that uses a 13.5 nm wavelength light source instead of a 193 nm wavelength ArF light source was applied to implement a finer pattern.[9–12] EUV lithography has a higher resolution due to its shorter wavelength, so it has the advantage of being able to implement the same line width with fewer process steps and less cost without using multi-patterning.

However, there are several problems in applying EUV lithography to extend the process range. In the EUV light source, the energy of one photon is ~ 14 times stronger than that of the ArF light source. However, in EUV lithography, the number of photons per unit area is much fewer than that in DUV lithography.[13] For this reason, the thickness of the photoresist (PR) is getting thinner than ~ 50 nm in order to companste enough photons for reaction. And, due to the thin thickness of resist, high etch resistance of resist is required during the etching of underlayer (generally, a hardmask layer such as SiON). In addition, due to the large energy and smaller number of EUV photons compared to those of the ArF light source, the probability of the secondary electron generation from the resist by the EUV photons is discontinuous, causing the problem of increasing line edge roughness (LER).[12,14–16] The increased LER of EUV PR consequently leads to an increased LER of the hard mask, and eventually, it is transferred to the LER of device final pattern causing critical dimension (CD) uniformity variation, deterioration of the electrical characteristics of the device, etc.[17–20].

To relieve the problems related to the EUV PR, efforts have been made recently by increasing the etch resistance of PR patterns through research such as the selective area deposition method, which selectively deposits only the PR area in a plasma state, and the cyclic depo-etch method, which repeatedly proceeds deposition and etching.[21–23] However, these methods do not increase the fundamental durability of the PR but increase the thickness, and add a deposition process to compensate for the shortcomings, leading to a burden of increased cost and time.

Previously, research on treating nanometer-scale block copolymers

* Corresponding author.
E-mail address: gyyeom@skku.edu (G.Y. Yeom).

https://doi.org/10.1016/j.apsusc.2023.157439
Received 6 February 2023; Received in revised form 11 April 2023; Accepted 29 April 2023
Available online 5 May 2023

(BCP) with sulfur-containing plasmas before the etching process was conducted, and it was found that, after the treatment with a sulfur-containing plasma of H_2S, the pattern stability and etch resistance during the etching with fluorocarbon plasmas were improved.[24] Sulfur is used for doping carbon-based materials by atomic substitution of crystal lattice, surface functionalization, etc., and applied studies on modifying physical and chemical properties of carbon materials have been reported.[25–30] Therefore, in this study, a possibility of transferring EUV PR pattern to underlayers without deformation of resist during the etching was investigated through a CS_2 plasma treatment containing sulfur and heat treatment of developed EUV PR. The etching was performed using a CF_4 plasma, which is used to etch the hardmask material such as SiON, and the changes in residual thicknesses of EUV resist, line edge roughness (LER), and critical dimension (CD) were compared before and after the treatments.

2. Experimental details

Fig. 1 (a) shows the overall process of the CS_2 plasma treatment for the hardening of EUV PR. Using EUV PR (reference) formed on a silicon wafer, CS_2 plasma treatments were performed using an inductive coupled plasma (ICP) type plasma shown in Fig. 1 (b) without biasing the substrate at room temperature. For the CS_2 plasma treatment, 13.56 MHz RF power in the range of 50 to 500 W was applied to the ICP source while keeping 9 mTorr of CS_2 gas pressure. The CS_2 plasma treatment time was varied from 30 *sec* to 10 min, and the treatment effect was compared with the reference. The annealing of the reference and CS_2 plasma treated EUV PR was performed on a hot plate at a temperature ranging from 40 to 200 ℃ for 15 min. The variously treated EUV PR samples were etched with a CF_4/Ar plasma used for the hard mask etching such as SiON by a reactive ion beam etcher(RIBE) shown in Fig. 1 (c). For the etching of EUV PR using the RIBE system, 1000 W of 13.56 MHz RF power was applied to the ICP source with 3 mTorr of CF_4: Ar (1:10) while applying 50 V to the 1st grid, −50 V to the 2nd grid, and ground potential to the 3rd grid. The pattern EUV photoresist was etched for 40 s.

As EUV samples, a silicon wafer (SK Siltron; p-type, ⟨1 0 0⟩, boron-doped, 10 O-cm silicon) blankly coated with a ~ 50 nm thick negative-tone type chemical amplified resist(CAR) was used to measure the etch depths after the CF_4/Ar plasma, and for the surface analysis before and after the surface treatments using CS_2 plasma and annealing. For the measurement of the change in LER (ΔLER) and the change in CD (ΔCD), the same EUV resist coated on a bottom antireflective coating (BARC) layer was patterned to have ~ 150 nm wide line patterns by using a KrF lithography equipment (the negative-tone EUV PR used in this experiment could be patterned with KrF lithography).

The changes in EUV photoresist after the etching with a CF_4/Ar plasma such as etch depth, etch profile, LER, and CD were observed using a field emission scanning microscope (FE-SEM; Hitachi, S-4700). The variations in LER and CD (ΔLER and ΔCD) were measured with a MATLAB-based software: Line and Contact Edge Roughness Meter (LACERM). To confirm the surface treatment effects, the chemical bonding state and atomic % of EUV photoresist before and after the CS_2 plasma treatment and/or annealing were investigated by X-ray photoelectron spectroscopy (XPS; Thermo VG, MultiLab 2000). In addition, Fourier transform infrared spectroscopic analysis (FT-IR; Bruker, IFS-66/S, TENSOR 27) was performed to analyze the structural changes and types of bonds in photoresist before and after the surface treatment. The dissociated species of the CS_2 plasma were observed using optical emission spectroscopy (OES; Andor, iStar734).

3. Results and discussion

Fig. 2 shows the remaining thickness of blank EUV PR after surface treatments, annealing, and etching measured as a function of (a) CS_2 plasma power, (b) annealing temperature, and (c) CS_2 plasma treatment time to find out the optimum surface treatment condition for the CS_2 plasma treatment time and annealing temperature. In Fig. 2 (a), the CS_2 plasma was operated at 9 mTorr CS_2 and the treatment time was 2 min, the annealing was performed at 80 °C for 15 min after the CS_2 plasma treatment, and etching was carried out after the CS_2 plasma treatment + annealing for 40 *sec* using RIBE with 3 mTorr of CF_4/Ar (1:10) while applying 1000 W of ICP power, 50 V of 1st grid voltage, and −50 V of 2nd grid voltage. The etching condition corresponds to the process

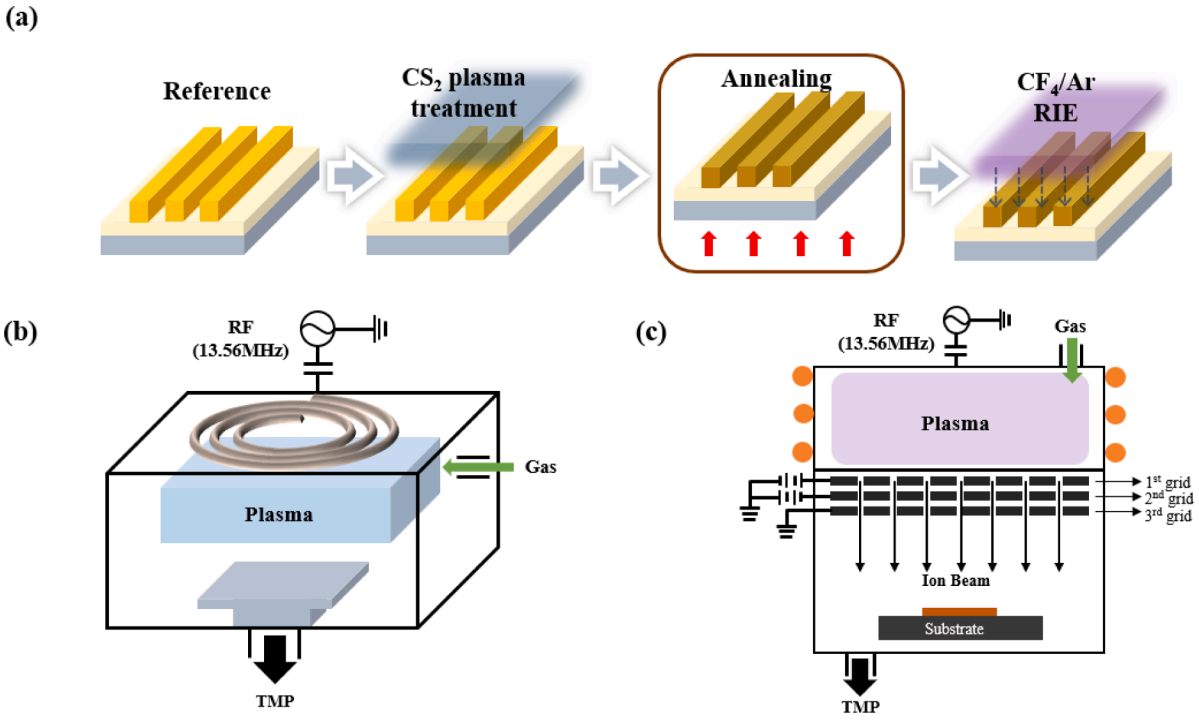

Fig. 1. Schematic diagrams of (a) overall EUV PR treatment process, (b) ICP system used in the CS_2 plasma treatment, and (c) RIBE system used in the etching.

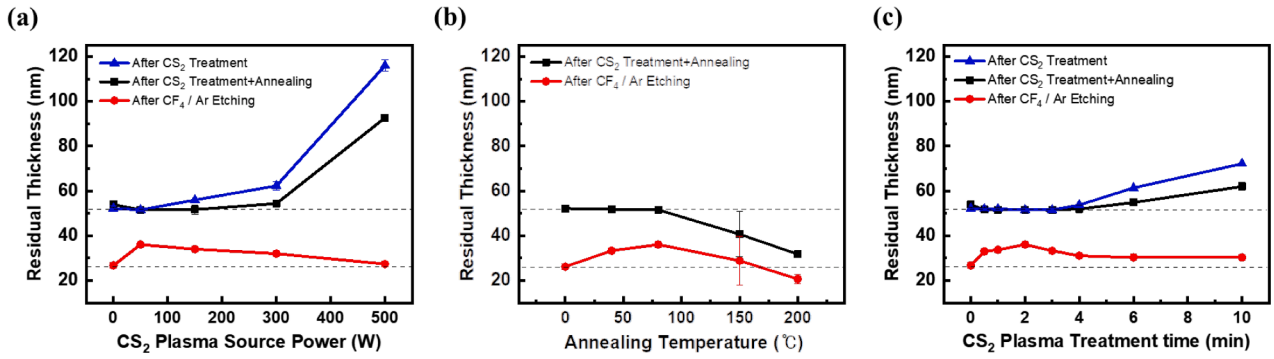

Fig. 2. EUV PR thickness after surface treatments, annealing, and etching measured as a function of (a) CS_2 plasma power, (b) annealing temperature, and (c) CS_2 plasma treatment time. In (a), the CS_2 plasma was operated at 9 mTorr CS_2 and the treatment time was 2 min, the annealing was performed at 80 °C for 15 min after the CS_2 plasma treatment. In (b), for the CS_2 plasma treatment, rf power was maintained at 50 W and the annealing time was kept at 15 min. In (c), the CS_2 plasma power was kept at 50 W and the annealing after the CS_2 plasma treatment at 80 ℃ for 15 min. Etching was carried out with 3 mTorr of CF_4/Ar (1:10) and the etching condition corresponds to the process condition of etching 20 nm thick SiON.

condition of etching 20 nm thick SiON. As shown in Fig. 2 (a), for the CS_2 plasma treatment, when the rf power was ≤ 50 W, no change in the thickness of EUV PR was observed, however, when the rf power was ≥ 150 W, increase of resist thickness was observed possibly due to the formation of CS polymer on the EUV PR surface, and the increase of the rf power increased the polymer thickness. When the EUV PR samples treated with CS_2 plasma at different rf power conditions were annealed at 80 °C for 15 min, no change in resist thickness was also observed for the EUV PR treated at ≤ 50 W of rf power. However, for the EUV PR treated at ≥ 150 W of rf power, the resist thickness was decreased slightly after annealing possibly due to the evaporation as CS_2 on the EUV PR surface. When the EUV PR samples treated with CS_2 plasma + annealing was etched using the etch condition described above, the increased remaining resist thickness was observed for 50 W of the CS_2 plasma power by showing 36.1 nm remaining resist thickness compared to 26.2 nm for the reference (from ~ 50 nm). However, the treatment at the higher CS_2 plasma powers (≥150 W) decreased the remaining resist thickness after the etching (34 nm for 150 W, 32 nm for 300 W, and 27.4 nm for 500 W) even though the remaining thicknesses were still thicker than that of the reference.

In Fig. 2 (b), the effect of annealing temperature on the remaining EUV PR thickness after annealing and etching is shown. For the CS_2 plasma treatment, rf power was maintained at 50 W and, during the annealing after the CS_2 plasma treatment, the annealing time was kept at 15 min. For annealing, up to 80 °C for 15 min, no change in resist thickness was observed, however, the increased annealing temperature of ≥ 150 °C decreased the resist thickness below the original EUV PR thickness (after 150 ℃ treatment, 40.7 nm, and, after 200 ℃ treatment, 31.8 nm). In fact, the reference EUV PR thickness was also decreased in similar thickness when annealed at ≥ 150 °C, therefore, the decrease of CS_2 plasma treated EUV PR at the higher temperature was not related to the CS_2 plasma treatment but the vaporization of the original EUV PR by annealing. In the case of the remaining EUV PR thickness after the CF_4/Ar etching, the increasing remaining resist thickness with increasing annealing temperature (33.3 nm for 40 ℃ treatment and 36.1 nm for 80 ℃) was observed up to 80 ℃, but the remaining resist thickness was decreased after the annealing ≥ 150 °C (at 150 ℃, 28.8 nm, and at 200 ℃, 20.7 nm). In fact, the decreased remaining resist thickness at the annealing temperature ≥ 150 °C was related to the thinner resist thickness after the annealing and, the amount of etch was continuously decreased with increasing annealing temperature (at 80 ℃, 15.5 nm, 150 ℃, 11.9 nm, and at 200 ℃, 11.1 nm) possibly indicating the formation of more strong bonding of sulfur with EUV PR. However, because the final remaining resist thickness was the thickest at 80 ℃, it was selected as an optimum condition for annealing.

In Fig. 2 (c), the effect of the CS_2 plasma treatment time on the remaining resist thickness is shown while keeping the CS_2 plasma power at 50 W and the annealing after the CS_2 plasma treatment at 80 ℃ for 15 min. As shown in Fig. 2 (c), no change in resist thickness was observed until 3 min of CS_2 plasma treatment, however, the further increase of CS_2 plasma treatment time up to 10 min increased resist thickness slowly possibly the CS polymer deposition on the EUV PR surface. The increased resist thickness caused by the deposition was slightly decreased after the annealing process. And, after the CF_4/Ar etching using the condition in Fig. 2 (a), the remaining resist thickness was increased up to 2 min CS_2 plasma treatment (after 30 *sec*, 33 nm; after 1 min, 33.7 nm; after 2 min, 36.1 nm), however, the further increased CS_2 plasma treatment time decreased the remaining resist thickness (after 3 min, 33.3 nm; after 4 min, 31.1 nm; after 6 min, 31.1 nm; after 10 min, 30.3 nm). Therefore, by using the optimum condition of CS_2 plasma treatment at 50 W for 2 min and annealing at 80 °C for 15 min, the etch amount of EUV PR was decreased from 26 nm (for reference; PR thickness decreased from 52.2 to 26.2 nm after etching) to 15.5 nm (for CS_2 + Annealing; PR thickness decreased from 51.6 nm to 36.1 nm after etching), therefore, the improvement of etch resistance of ~ 70 % could be achieved.

Using patterned EUV PR samples with the pattern width of ~ 150 nm (143 ~ 151 nm) after the KrF lithography, the changes of critical dimension (ΔCD) and line edge roughness (ΔLER) were measured with a MATLAB-based software described in the experimental section before and after the etching of EUV PR treated with CS_2 plasma only, annealing only, CS_2 plasma + annealing in addition to the reference using the optimized conditions described above and the results are shown in Fig. 3 (a) for ΔLER and (b) for ΔCD. The changes in the EUV PR thickness (ΔThickness) for the patterned EUV PR before and after the etching were also observed using FE-SEM, and the results are shown in Fig. 3 (c). (Thickness information of each treatment condition is shown in Figure S1.) The etch condition was the same as the condition in Fig. 2 (a). As shown in Fig. 3 (c), the etched amount of the patterned EUV PR was similar to the blank EUV PR by showing ~ 26 nm for the reference and ~ 15 nm for the resist treated with CS_2 plasma + annealing. In addition, the resist treated with the annealing only showed ΔThickness of ~ 28 nm and that treated with the CS_2 plasma only showed ΔThickness of ~ 18.8 nm, therefore, the annealing itself did not improve the etch resistance of EUV PR and the CS_2 plasma treatment only also showed the etch resistance of EUV PR even though the following annealing improved the etch resistance more. As shown in Fig. 3 (a) and (b), the improvement of ΔLER and ΔCD was also observed after the CS_2 plasma treatment and further improvement after the CS_2 plasma treatment + annealing while no improvement was observed after the annealing only (ΔLER/ΔCD: 3.22/-15.8 nm for reference, 3.15/-21 nm for annealing, 0.9/-5.4 nm for CS_2 plasma only, and 0.3/-0.2 nm for CS_2

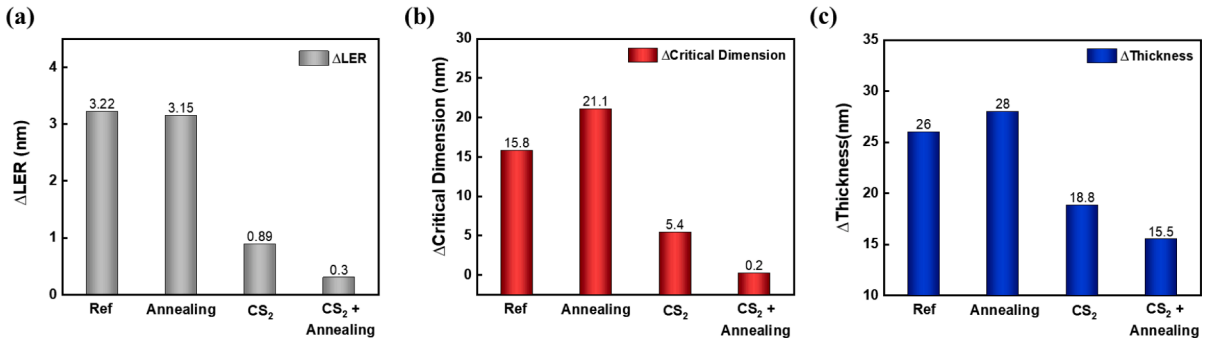

Fig. 3. (a) LER (ΔLER) (b) CD (ΔCD), and (c) Thickness(ΔThickness) of EUV PR after the etching of EUV PR treated with CS_2 plasma only, annealing only, CS_2 plasma + annealing in addition to the reference. CS_2 plasma treatment condition: 9mTorr CS_2, 50 W and 2 min. Annealing condition: 80 °C for 15 min. The etching condition is the same as the optimized conditions in Fig. 2.

plasma + annealing). Fig. 4 shows the top-down FE-SEM images of patterned EUV PR samples before and after etching with a RIBE system for (a) reference, (b) after annealing only (c) after CS_2 plasma treatment only, and (d) after CS_2 plasma treatment + annealing. As shown in Fig. 4 (d), no significant changes in ΔLER and ΔCD were observed after the etching for the EUV PR treated with the CS_2 plasma + annealing while significant increase of LER and decrease of CD were observed for both reference EUV PR and annealed EUV PR. (A conventional reactive ion etching system was also used in the etching of EUV PR before and after the treatments, and the same trends were observed. See supplementary information Figure S2 and Table S1.).

To understand the location of surface treatment effect, the reference resist and the resists treated with CS_2 plasma only/with CS_2 plasma + annealing were etched partially in depth and measured etch rate with depth and the results are shown in Fig. 5. As shown in Fig. 5, initially, at the surface of EUV PR, the etch rate of the reference was the highest (~1.1 nm/s) and that of resist treated with CS_2 plasma + annealing was the lowest (~0.5 nm/s) while the resist treated with CS_2 plasma only showed the etch rate of ~ 0.8 nm/s. The differences were decreased with depth and, at the etched thickness of ~ 25 nm, the etch rate of the CS_2 plasma treated resist was similar to that of reference, and, at the etched thickness of ~ 40 nm, the etch rates of CS_2 plasma treated resist, CS_2 plasma treated resist, and reference became similar. Therefore, it is believed that, ~ 25 nm thick EUV PR is affected by the CS_2 plasma treatment and ~ 40 nm by the annealing at 80 ℃ after the CS_2 plasma treatment.

The species forming in the plasma during the CS_2 plasma treatment were observed using OES for the optimized condition of 9 mTorr CS_2 and 50 W of ICP source power and the results are shown in Fig. 6 (a) for the wide wavelength range from 200 ~ 900 nm and (b) for the narrow wavelength range of 200 ~ 300 nm and 400 ~ 600 nm. As shown in Fig. 6 (a), sharp peaks at 200 ~ 300 nm and a broad peak at 400 ~ 600 nm were observed and, the detailed investigation of peaks showed that, as shown in Fig. 6 (b), the broad peak at 400 ~ 600 nm was related to the CS_2 vibrational peaks[31,32] while the sharp peaks at 200 ~ 300 nm were mostly related to the CS and S which were dissociated from CS_2. Therefore, it is found out that the EUV PR surface is affected by dissociated species such as CS and S. (The EUV PR was not affected by gaseous CS_2 itself. See Supplementary information Figure S3; there was no chemical changes of EUV PR surface when the EUV PR was exposed to gaseous CS_2 only.).

The surface composition and binding states of EUV PR surface before and after annealing and/or CS_2 plasma treatment were investigated by XPS and the results are shown in Fig. 7 (a) for the surface composition, (b) narrow scan data of sulfur 2p peak, and (c) narrow scan data of carbon 1 s peak. The process conditions are the same as the optimized conditions of Fig. 2. As shown in Fig. 7 (a), after the annealing only, no differences in surface composition were observed (C:O:S:F:I = 78:16:1:4:1% for reference, and 77:17:1:4:1% for annealed). However, after the CS_2 plasma treatment, the increased sulfur percentage from 1 to 37 % (C:O:S:F:I = 52:8:37:1:0.3 %) was observed and the annealing after the CS_2 plasma treatment decreased the sulfur percentage to 32 % (C:O:S:F:I = 56:10:32:2:0.2 %). In the XPS narrow scan data of S 2p peak, as shown in Fig. 7 (b), the increased sulfur showed -C—S—C- related peaks

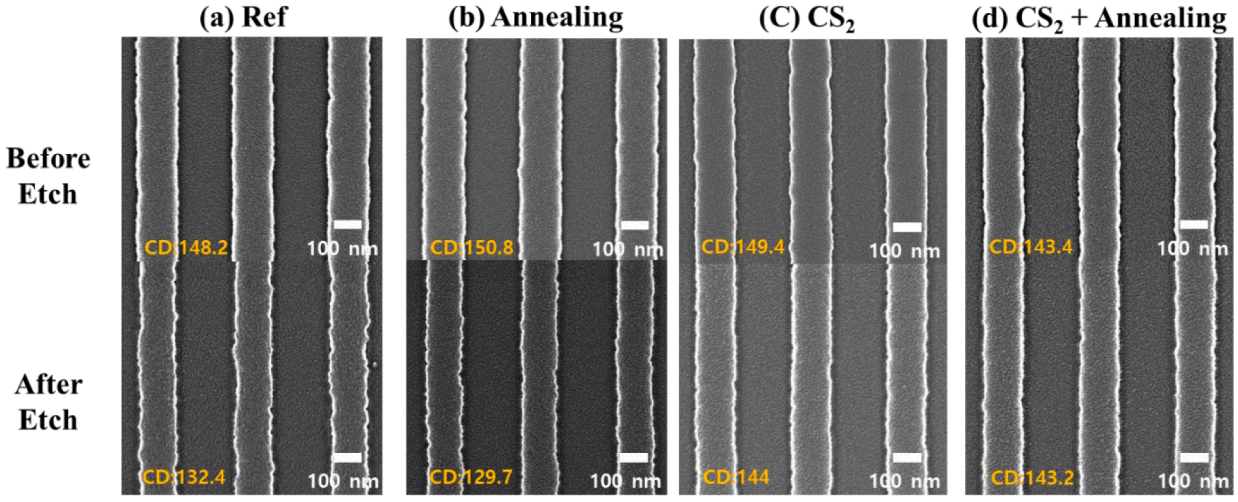

Fig. 4. Top-down FE-SEM images of patterned EUV PR samples before and after etching with a RIBE system for (a) reference, (b) after annealing only (c) after CS_2 plasma treatment only, and (d) after CS_2 plasma treatment + annealing in Fig. 3.

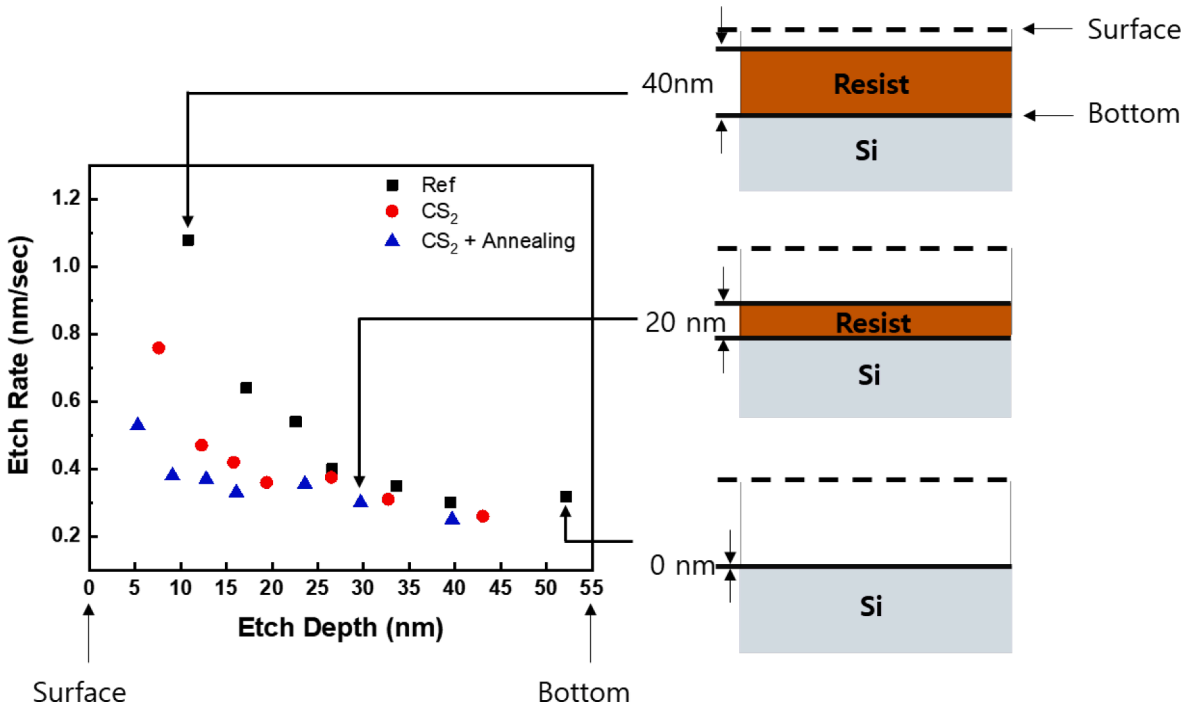

Fig. 5. Etch rate with depth of the reference resist and the resists treated with CS_2 plasma only and with CS_2 plasma + annealing. The process conditions are the same as those in Fig. 3.

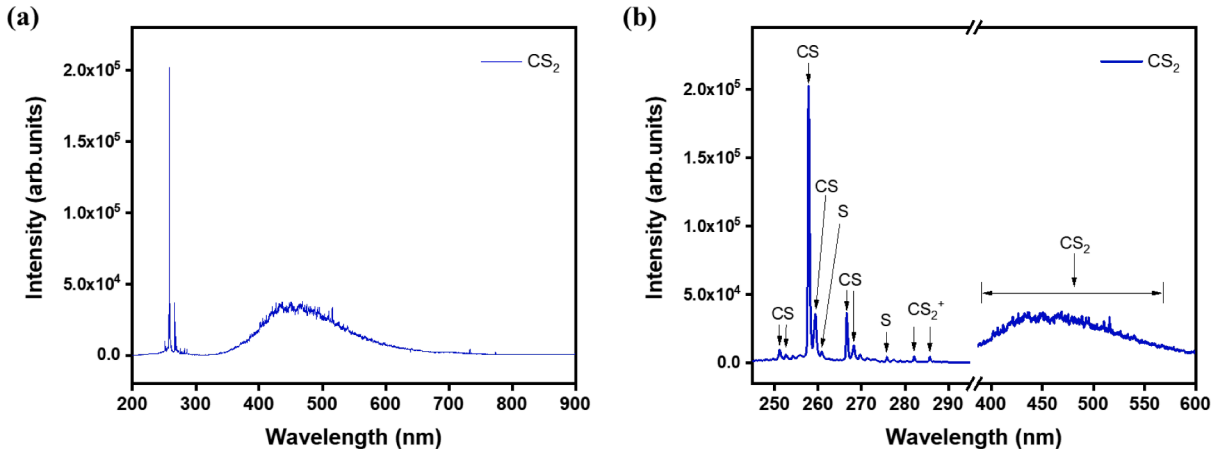

Fig. 6. OES data of CS_2 plasma for the optimized condition of 9 mTorr CS_2 and 50 W of ICP power. (a) is for the wide wavelength range from 200 ~ 900 nm and (b) for the narrow wavelength range of 200 ~ 300 nm and 400 ~ 600 nm.

by showing shifted S $2p_{3/2}$ and S $2p_{1/2}$ peaks at 163.8 (from 163.2 eV for sulfur only) and 165.1 eV (164.7 eV for sulfur only), respectively. In addition, the small peaks related to -C—$S(O)_x$-C-, that is, oxide sulfur peaks at 166.1 and 168.2 eV could be observed.[33,34] In the case of XPS narrow scan data of C 1 s peak, as shown in Fig. 7 (c), due to the same bonding peaks of C—C and C—S at ~ 284.6 eV, no additional peak could be observed on C 1 s peak by the increase of sulfur on EUV PR surface. To understand the effect of annealing after the CS_2 plasma treatment, when the ratio of S—O bonding area/C—S bonding area was taken from Fig. 7 (b), the slight increased ratio of 0.156 for the CS_2 plasma treatment + annealing from 0.147 for the CS_2 plasma treatment was observed, therefore, S—O bonds appeared to be increased somewhat in the resist after the annealing.

To understand the effect of annealing after the CS_2 plasma treatment, XPS depth profiling was carried out with an Ar^+ ion beam for the CS_2 plasma treated resist and the annealed resist after the CS_2 plasma treatment and the results are shown in Fig. 8 (a) for the composition ratios of CS_2 plasma treated resist and (b) for those of the resist treated with CS_2 plasma + annealing with Ar^+ ion depth profiling time. The process conditions are the same as the optimized conditions in Fig. 2. As shown in Fig. 8 (a) and (b), both resists showed the decrease of sulfur with increasing depth profiling from the resist surface, however, the resist treated with the CS_2 plasma showed faster decrease of sulfur content in the resist with depth compared to that treated with the CS_2 plasma + annealing. Fig. 8 (c) shows the changes in sulfur percentages with depth shown in Fig. 8 (a) and (b), and, even though the sulfur composition was lower at the surface for the resist treated with CS_2 plasma + annealing (37 % for the CS_2 plasma treated and 32 % for the CS_2 plasma + annealing), the decrease in sulfur content with depth was slower than that treated with the CS_2 plasma, therefore, the sulfur percentage was remaining higher at the similar depth in the resist. Therefore, it is believed that the higher etch resistance observed after the

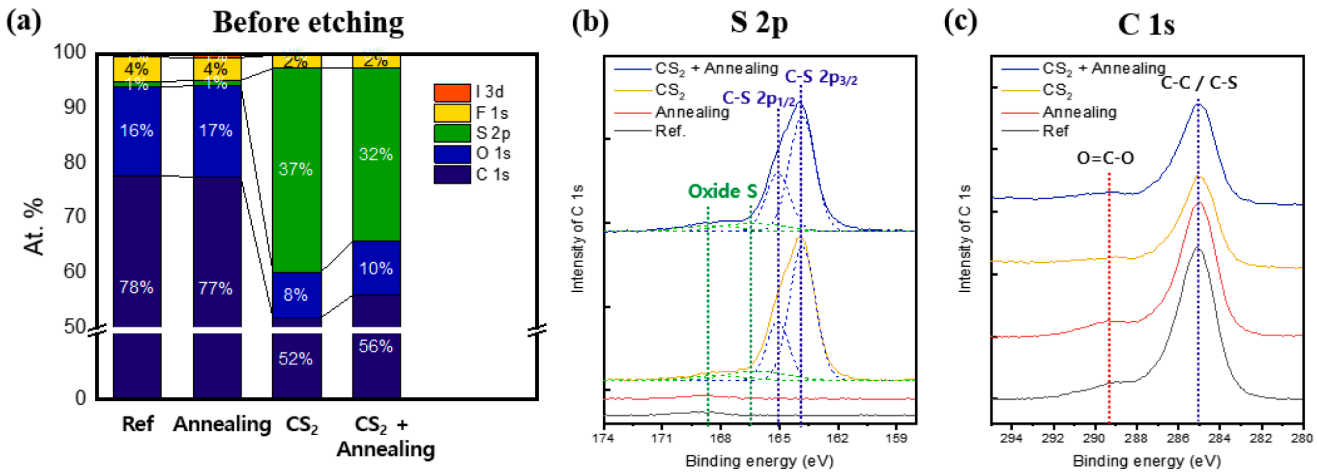

Fig. 7. Surface composition and binding states of EUV PR surface before and after annealing and/or CS_2 plasma treatment by XPS. (a) the surface composition, (b) narrow scan data of sulfur 2p peak, and (c) narrow scan data of carbon 1 s peak.

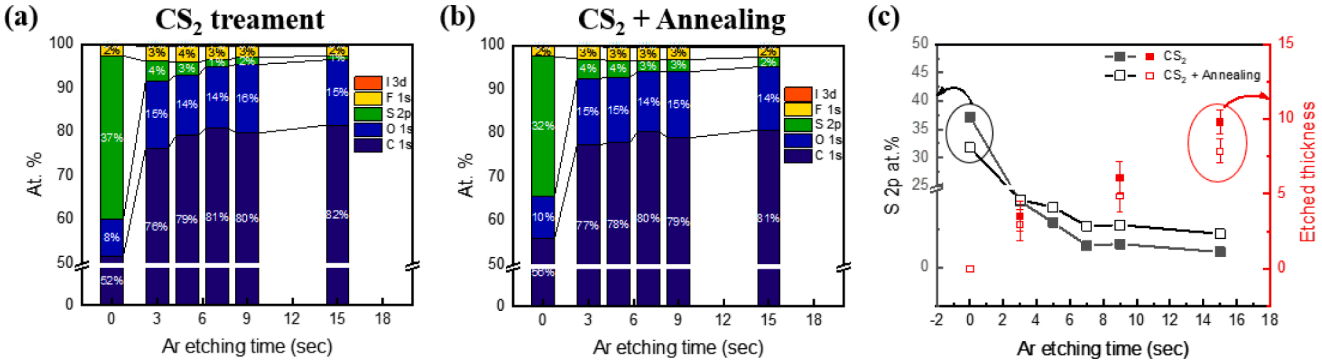

Fig. 8. XPS depth profiling with an Ar^+ ion for the CS_2 plasma treated resist and the annealed resist after the CS_2 plasma treatment. (a) the composition ratios of CS_2 plasma treated resist and (b) those of the resist treated with CS_2 plasma + annealing with Ar^+ ion depth profiling time. (c) Changes in sulfur percentages with depth shown in (a) and (b).

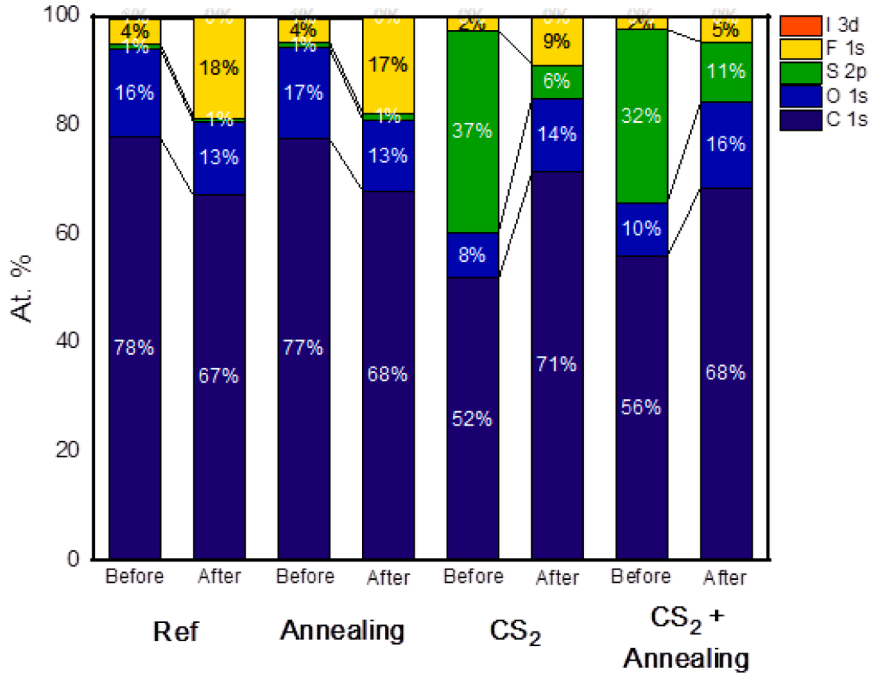

Fig. 9. Change in surface composition of the resist after the etching of 3 nm resist thickness using a CF_4/Ar plasma measured by XPS.

annealing of CS_2 plasma treated EUV PR appears be partially related to the increased diffusion of sulfur into the resist during the annealing. (Additional XPS narrow scan data for each condition are shown in Figure S4 and Figure S5.).

In addition to the surface analysis after the surface treatments, the change in surface composition of the resist after the etching was investigated using XPS and the results are shown in Fig. 9 for the resist samples treated by annealing, CS_2 plasma, and CS_2 plasma + annealing in addition to the reference. The process conditions are the same as the optimized conditions in Fig. 2. The resist etch depth using CF_4/Ar plasma was maintained at ~ 3 nm. As shown in Fig. 9, the reference and annealed resist showed the similar compositional changes before and after the etching, and the increase of F from 4 to 17 ~ 18 % could be observed while showing similar sulfur percentage of 1 % after the etching. In the case of the resist samples treated with CS_2 plasma and CS_2 plasma + annealing, significant decrease in sulfur percentage (S: from 37 to 6 % for CS_2 plasma treated and, from 32 to 11 % for CS_2 plasma treated + annealed) was observed, however, more sulfur content was observed on the resist treated with CS_2 plasma + annealing. Especially, in case of fluorine, even though the F content was increased after the etching for both resist treated with CS_2 plasma and CS_2 plasma + annealing (F: from 2 to 9 % for CS_2 plasma treated and from 2 to 5 % for CS_2 plasma treated + annealed), the F percentages were smaller compared to those of the reference and annealed and, the F percentage of the resist treated with CS_2 plasma + annealing was also smaller than that treated with CS_2 plasma. That is, higher the sulfur on the resist, lower the fluorine on the resist, therefore, it appears that, the reaction of resist with fluorine in the CF_4/Ar plasma is disturbed by sulfur on the EUV PR surface, and, it increases the etch resistance of the CS_2 plasma treated resist. (Additional XPS narrow scan data for after etching by CF_4/Ar plasma condition are shown in Figure S6.) In addition, the formation of bonds such as S═O and C═S which have higher bonding energy than single bonding or C—C bonding after applying an annealing process after the CS_2 plasma treatment as shown in Figs. 7 and 10 appears to contribute to the hardening of EUV PR even though it is difficult to find out which bonds contribute the hardening of PR.

The binding states of EUV PR before and after the treatments were also investigated using FT-IR. Fig. 10 (a) shows transmittance results of FT-IR for the EUV PR after annealing, CS_2 plasma treatment, and CS_2 plasma treatment + annealing in addition to the reference. The process conditions were the same as the optimized conditions in Fig. 2. As shown in Fig. 10 (a), The absorption peaks were similar, however, there were some differences in wavenumber range of 1100 ~ 1400 cm^{-1}. To figure out the differences, the FT-IR data of the EUV PR after annealing, CS_2 plasma treatment, and CS_2 plasma treatment + annealing were subtracted by that of reference and the results are shown in Fig. 10 (b) for the wavenumber range of 1050 ~ 1550 cm^{-1}. The black line is the graph of annealed PR subtracted by that of the reference, and no noticeable differences were observed between the reference and annealed EUV. The graph of CS_2 plasma treated subtracted by the reference showed a peak at 1160 cm^{-1} related to O═S = O binding and C—S binding. After the annealing of CS_2 plasma treated resist, in addition to the peak related to O═S = O binding and C—S binding, the peaks related to S═O (near 1400 cm^{-1}) and C═S (near 1080 and 1280 cm^{-1}) were observed. [35–38] Therefore, it is believed that the sulfur on the EUV PR after the CS_2 plasma treatment forms new bonding with carbon such as C—S in the resist preventing the reaction with fluorine and further bonding such as S═C and S═O contributing hardening of PR after the annealing in addition to the diffusion of sulfur into the resist, and which appears to strengthen the etch resistance of the EUV PR after the CS_2 plasma treatment and CS_2 plasma treatment + annealing.

4. Conclusions

In this study, the effect of CS_2 plasma treatment and annealing on surface hardening of EUV photoresist was investigated. After the CS_2 plasma treatment at 50 W ICP power for 2 min followed by annealing at 80 ℃ for 15 min, the etch resistance of EUV PR was increased by ~ 70 % compared to the reference PR. In addition, after the CS_2 treatment and annealing, ΔLER and ΔCD of the patterned EUV PR were significantly decreased. The improvement of EUV PR properties after the CS_2 plasma treatment was appeared to be related to the formation of C—S bonding on the surface and the further improvement of EUV PR properties after the annealing was related to the formation of C═S bonding and S═O bonding in addition to the diffusion of sulfur into the resist. That is, after CS_2 treatment and annealing, new bonds related to S were formed and the bond strength was increased after the annealing in addition to diffusion, and which appears to be related to improvement of etch resistance by preventing the reaction with F or CF_x during the etching with CF_4/Ar. In conclusion, the surface hardening of EUV photoresist can be achieved without thickness change and with a simple process, and the results can be applied as a next-generation process to improve etch resistance of EUV PR.

CRediT authorship contribution statement

Won Jun Chang: Conceptualization, Methodology, Investigation, Validation, Writing – original draft. **Hee Ju Kim:** Conceptualization,

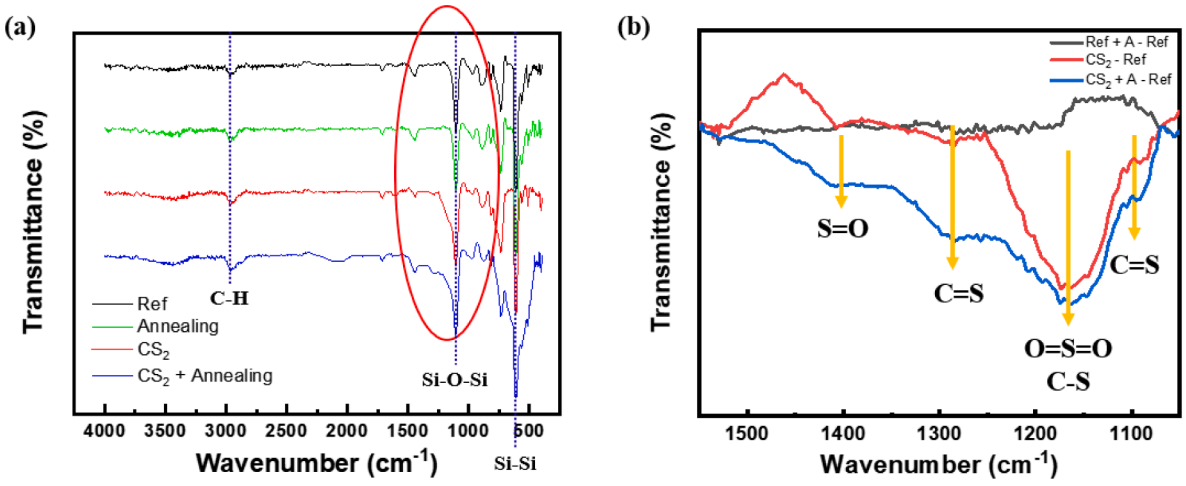

Fig. 10. FT-IR data on binding states of EUV PR before and after the treatments. (a) transmittance results of FT-IR for the EUV PR after annealing, CS_2 plasma treatment, and CS_2 plasma treatment + annealing in addition to the reference. (b) FT-IR data of (a) subtracted by that of reference for the wavenumber range of 1050 ~ 1550 cm^{-1}.

Methodology, Investigation, Writing – review & editing. **Geun Young Yeom:** Supervision, Writing – review & editing.

Declaration of Competing Interest

The authors declare that they have no known competing financial interests or personal relationships that could have appeared to influence the work reported in this paper.

Data availability

Data will be made available on request.

Acknowledgments

This work was supported by Nano Material Technology Development Program through the funded by the Ministry of Education, Science and Technology (2021M3H4A1A02055667). And thanks to Dongwoo Fine-Chem for providing EUV resist wafers.

Appendix A. Supplementary data

Supplementary data to this article can be found online at https://doi.org/10.1016/j.apsusc.2023.157439.

References

[1] A. Pimpin, W. Srituravanich, Reviews on micro- and nanolithography techniques and their applications, Engineering Journal. 16 (2012) 37–55, https://doi.org/10.4186/ej.2012.16.1.37.
[2] R.H. Stulen, D.W. Sweeney, Extreme ultraviolet lithography, IEEE J Quantum Electron. 35 (1999) 694–699, https://doi.org/10.1109/3.760315.
[3] R.F. Pease, S.Y. Chou, Lithography and other patterning techniques for future electronics, Proc. IEEE 96 (2008) 248–270, https://doi.org/10.1109/JPROC.2007.911853.
[4] L.F. Thompson, Introduction to Microlithography, 1983. https://pubs.acs.org/sharingguidelines.
[5] P. Xu, Y. Chen, Y. Chen, L. Miao, S. Sun, S.-W. Kim, A. Berger, D. Mao, C. Bencher, R. Hung, C. Ngai, Sidewall spacer quadruple patterning for 15nm half-pitch, in: Optical Microlithography XXIV, SPIE, 2011, p. 79731Q, https://doi.org/10.1117/12.881547.
[6] H. Nakagawa, T. Fujisawa, K. Goto, T. Kimura, T. Kai, Y. Hishiro, Ultra-thin-film EUV resists beyond 20nm lithography, in: Advances in Resist Materials and Processing Technology XXVIII, SPIE, 2011, p. 79721I, https://doi.org/10.1117/12.879303.
[7] W.H. Arnold, M. Dusa, J. Flinders, Metrology challenges of double exposure and double patterning, in: Metrology, Inspection, and Process Control for Microlithography XXI, SPIE, 2007, p. 651802, https://doi.org/10.1117/12.721459.
[8] C. Bencher, Y. Chen, H. Dai, W. Montgomery, L. Huli, 22nm half-pitch patterning by CVD spacer self alignment double patterning (SADP), in: Optical Microlithography XXI, SPIE, 2008, p. 69244E, https://doi.org/10.1117/12.772953.
[9] T.-S. Eom, H.-I. Kim, C.-K. Kang, Y.-J. Ryu, S.-H. Hwang, H.-H. Lee, H.-Y. Lim, J.-S. Park, N.-J. Kwak, S. Park, Patterning challenges of EUV lithography for 1X-nm node DRAM and beyond, in: Extreme Ultraviolet (EUV) Lithography IV, SPIE, 2013, p. 86791J, https://doi.org/10.1117/12.2011687.
[10] D. Ha, C. Yang, J. Lee, S. Lee, S.H. Lee, K.I. Seo, H.S. Oh, E.C. Hwang, S.W. Do, S. C. Park, M.C. Sun, D.H. Kim, J.H. Lee, M.I. Kang, S.S. Ha, D.Y. Choi, H. Jun, H. J. Shin, Y.J. Kim, J. Lee, C.W. Moon, Y.W. Cho, S.H. Park, Y. Son, J.Y. Park, B. C. Lee, C. Kim, Y.M. Oh, J.S. Park, S.S. Kim, M.C. Kim, K.H. Hwang, S.W. Nam, S. Maeda, D.W. Kim, J.H. Lee, M.S. Liang, E.S. Jung, Highly manufacturable 7nm FinFET technology featuring EUV lithography for low power and high performance applications, in: Digest of Technical Papers - Symposium on VLSI Technology, Institute of Electrical and Electronics Engineers Inc., 2017, pp. T68–T69, https://doi.org/10.23919/VLSIT.2017.7998202.
[11] M. Neisser, S. Wurm, ITRS lithography roadmap: 2015 challenges, Advanced Optical Technologies. 4 (2015) 235–240, https://doi.org/10.1515/aot-2015-0036.
[12] A. Lio, EUV resists: What's next?, in: Extreme Ultraviolet (EUV) Lithography VII SPIE, 2016, p. 97760V, https://doi.org/10.1117/12.2225017.
[13] P. Dentinger, G. Cardinale, C. Henderson, A. Fisher, A. Ray-Chaudhuri, Photoresist Film Thickness for Extreme Ultraviolet Lithography, in: Emerging Lithographic Technologies IV, SPIE, 2000, https://doi.org/10.1117/12.390098.
[14] M. Trikeriotis, M. Krysak, Y.S. Chung, C. Ouyang, B. Cardineau, R. Brainard, C. K. Ober, E.P. Giannelis, K. Cho, A new inorganic EUV resist with high-etch resistance, in: Extreme Ultraviolet (EUV) Lithography III, SPIE, 2012, p. 83220U, https://doi.org/10.1117/12.916384.
[15] J.M. Hutchinson, The Shot Noise Impact on Resist Roughness in EUV Lithography, n.d. http://proceedings.spiedigitallibrary.org/.
[16] P. de Bisschop, J. van de Kerkhove, J. Mailfert, A. Vaglio Pret, J. Biafore, Impact of stochastic effects on EUV printability limits, in: Extreme Ultraviolet (EUV) Lithography V, SPIE, 2014, p. 904809, https://doi.org/10.1117/12.2047827.
[17] R.L. Brainard, P. Trefonas, J.H. Lammers, C.A. Cutler, J.F. Mackevich, A. Trefonas, S.A. Robertson, Shot noise, LER, and quantum efficiency of EUV photoresists, in: Emerging Lithographic Technologies VIII, SPIE, 2004, p. 74, https://doi.org/10.1117/12.536411.
[18] O. Wood, D.G. Seiler, A.C. Diebold, R. McDonald, C.M. Garner, D. Herr, R. P. Khosla, E.M. Secula, E.U.V. Lithography, New Metrology Challenges, in: AIP Conf Proc, AIP (2007) 375–381, https://doi.org/10.1063/1.2799401.
[19] T. Manouras, P. Argitis, High sensitivity resists for EUV lithography: A review of material design strategies and performance results, Nanomaterials 10 (2020) 1–24, https://doi.org/10.3390/nano10081593.
[20] C. Luo, C. Xu, L. Lv, H. Li, X. Huang, W. Liu, Review of recent advances in inorganic photoresists, RSC Adv. 10 (2020) 8385–8395, https://doi.org/10.1039/c9ra08977b.
[21] M. Mao, F. Lazzarino, P. de Schepper, D. de Simone, D. Piumi, V. Luong, F. Yamashita, M. Kocsis, K. Kumar, Patterning with metal-oxide EUV photoresist: patterning capability, resist smoothing, trimming, and selective stripping, in: Advances in Patterning Materials and Processes XXXIV, SPIE, 2017: p. 101460I. https://doi.org/10.1117/12.2258118.
[22] R. Nye, K. van Dongen, H. Oka, H. Furutani, G. Parsons, D. de Simone, A. Delabie, Improving polymethacrylate EUV resists with TiO_2 area-selective deposition, in, SPIE-Intl Soc Optical Eng (2022) 27, https://doi.org/10.1117/12.2613815.
[23] T. Wada, C.-Y. Hsieh, A. Ko, P. Biolsi, Line roughness improvements on EUV 36nm pitch pattern by plasma treatment method, in, SPIE-Intl Soc Optical Eng (2019) 18, https://doi.org/10.1117/12.2514764.
[24] S.W. Choi, J.H. Shin, M.H. Jeon, J.H. Mun, S.O. Kim, G.Y. Yeom, K.N. Kim, Surface modification of block copolymer through sulfur containing plasma treatment, J Nanosci Nanotechnol. 15 (2015) 8093–8098, https://doi.org/10.1166/jnn.2015.11286.
[25] V.K. Abdelkader-Fernández, M. Domingo-García, F.J. López-Garzón, D. M. Fernandes, C. Freire, M.D. López de la Torre, M. Melguizo, M.L. Godino-Salido, M. Pérez-Mendoza, Expanding graphene properties by a simple S-doping methodology based on cold CS_2 plasma, Carbon N Y. 144 (2019) 269–279, https://doi.org/10.1016/j.carbon.2018.12.045.
[26] W. Kiciński, M. Szala, M. Bystrzejewski, Sulfur-doped porous carbons: Synthesis and applications, Carbon N Y. 68 (2014) 1–32, https://doi.org/10.1016/J.CARBON.2013.11.004.
[27] M. Seredych, E. Rodríguez-Castellón, T.J. Bandosz, Alterations of S-doped porous carbon-rGO composites surface features upon CO_2 adsorption at ambient conditions, Carbon N Y. 107 (2016) 501–509, https://doi.org/10.1016/J.CARBON.2016.06.028.
[28] J.E. Park, Y.J. Jang, Y.J. Kim, M.S. Song, S. Yoon, D.H. Kim, S.J. Kim, Sulfur-doped graphene as a potential alternative metal-free electrocatalyst and Pt-catalyst supporting material for oxygen reduction reaction, PCCP 16 (2014) 103–109, https://doi.org/10.1039/c3cp54311k.
[29] W. Feng, E. Borguet, R.D. Vidic, Sulfurization of carbon surface for vapor phase mercury removal – I: Effect of temperature and sulfurization protocol, Carbon N Y. 44 (2006) 2990–2997, https://doi.org/10.1016/J.CARBON.2006.05.019.
[30] L. Chen, X. Cui, Y. Wang, M. Wang, R. Qiu, Z. Shu, L. Zhang, Z. Hua, F. Cui, C. Wei, J. Shi, One-step synthesis of sulfur doped graphene foam for oxygen reduction reactions, Dalton Trans. 43 (2014) 3420–3423, https://doi.org/10.1039/c3dt52253a.
[31] J. Gackowska, R. Olszewski, M. Zubek, Fluorescence emission of carbon disulfide in low-energy electron collisions, Radiat. Phys. Chem. 68 (2003) 133–136, https://doi.org/10.1016/S0969-806X(03)00268-8.
[32] M. Zubek, J. Gackowska, A. Snegursky, Dissociative excitation of carbon disulfide by electron impact, Radiat. Phys. Chem. 68 (2003) 323–328, https://doi.org/10.1016/S0969-806X(03)00309-8.
[33] H. Chen, F. Yu, G. Wang, L. Chen, B. Dai, S. Peng, Nitrogen and Sulfur Self-Doped Activated Carbon Directly Derived from Elm Flower for High-Performance Supercapacitors, ACS Omega 3 (2018) 4724–4732, https://doi.org/10.1021/acsomega.8b00210.
[34] L. Qie, W. Chen, X. Xiong, C. Hu, F. Zou, P. Hu, Y. Huang, Sulfur-Doped Carbon with Enlarged Interlayer Distance as a High-Performance Anode Material for Sodium-Ion Batteries, Adv. Sci. 2 (2015), https://doi.org/10.1002/ADVS.201500195.
[35] A.G. Hopkins, C.W. Brown, Infrared spectrum of sulfur monoxide, J Chem Phys. (1975) 2511–2512, https://doi.org/10.1063/1.430738.
[36] S. Baik, H. Zhang, Y.K. Kim, D. Harbottle, J.W. Lee, Enhanced adsorption capacity and selectivity towards strontium ions in aqueous systems by sulfonation of CO_2 derived porous carbon, RSC Adv. 7 (2017) 54546–54553, https://doi.org/10.1039/c7ra09541d.
[37] M. Shakirullah, I. Ahmad, M. Ishaq, W. Ahmad, Study on the role of metal oxides in desulphurization of some petroleum fractions, J. Chin. Chem. Soc. 56 (2009) 107–114, https://doi.org/10.1002/jccs.200900015.
[38] R. Kurniaty, K. Khairan, L. Lelifajri, ANALYSIS OF SILDENAFIL AND ITS DERIVATIVES IN JAMU (HERBAL MEDICINES) USING LC/MS/MS SPECTROSCOPY, Jurnal Natural. 18 (2018) 115–121. https://doi.org/10.24815/jn.v18i3.11153.